Influence of embedded indium nanocrystals on GaAs thermoelectric properties

M. V. Warren,[1] J. C. Canniff,[1] H. Chi,[2] E. Morag,[1,3] F. Naab,[4] V. A. Stoica,[2] R. Clarke,[2] C. Uher,[2] and R. S. Goldman[1,2]
[1]*Department of Materials Science and Engineering, University of Michigan, Ann Arbor, Michigan 48109, USA*
[2]*Department of Physics, University of Michigan, Ann Arbor, Michigan 48109, USA*
[3]*Huron High School, Ann Arbor, Michigan 48105, USA*
[4]*Department of Nuclear Engineering and Radiological Sciences, University of Michigan, Ann Arbor, Michigan 48109, USA*

(Received 5 June 2013; accepted 2 July 2013; published online 22 July 2013)

We have examined the formation of embedded In nanocrystals (NCs) and their influence on the free carrier concentration, resistivity, thermal conductivity, and Seebeck coefficient (S) of GaAs. The In nanocrystals enhance the free carrier concentration, while electron and phonon scattering at crystallite boundaries increases the resistivity and reduces the thermal conductivity. Furthermore, the room temperature Seebeck coefficient exhibits a 25% increase due to carrier trapping. Application of this approach to more heavily doped GaAs layers will likely lead to further increases in S and reductions in resistivity. © *2013 AIP Publishing LLC*. [http://dx.doi.org/10.1063/1.4816087]

I. INTRODUCTION

Nanocomposite materials have been identified as promising candidates for high figure-of-merit thermoelectric materials. Due to the increased control of the density of states and hence, the energies of charge carriers, nanocomposite materials are predicted to have a significantly higher thermoelectric figure-of-merit ($Z = S^2\sigma/\kappa$, where S is the Seebeck coefficient, σ is the electrical conductivity, and κ is the thermal conductivity) in comparison to their bulk counterparts.[1] For example, enhancements of Z due to low dimensionality have been reported for Bi_2Te_3/Sb_2Te_3 superlattices[2] and embedded Si nanocrystals in SiGe.[3] Additionally, it has been suggested that embedded metallic nanoparticles in a semiconducting matrix enhance its Seebeck coefficient via electron energy filtering.[4] Recently, a variety of embedded nanocrystals have been synthesized by matrix-seeded growth, which involves ion-beam-amorphization of a semiconductor film, followed by nanoscale recrystallization via rapid thermal annealing (RTA).[5,6] For the case of In^+ implantation into GaAs, a sputter-mask method was recently developed to maximize the retained ion dose by preventing sputtering, yielding an ion-fluence dependent $|S|$, with an enormous Seebeck coefficient of $-12\,mV/K$ at 4 K for a fluence of $3.8 \times 10^{17}\,cm^{-2}$. Furthermore, due to its highest retained In concentration, a fluence of $3.8 \times 10^{16}\,cm^{-2}$ was identified as most promising for the formation of embedded nanocomposites for thermoelectrics.[7] Here, we examine the influence of annealing temperature on the microstructure of the layers, identifying the formation mechanisms of In nanocrystals (NCs) embedded in polycrystalline GaAs. We discuss the influence of the In NCs and GaAs crystallite boundaries on the free carrier concentration, resistivity, Seebeck coefficient, and thermal conductivity of the layers. Indeed, the presence of In NCs leads to a maximum free carrier concentration of all annealed films and an increase in $|S|$ of $50\,\mu V/K$ at 300 K in comparison to that of an unimplanted film. The GaAs crystallite boundaries scatter both phonons and electrons, reducing σ by 80% and κ by 50%.

II. EXPERIMENTAL PROCEDURES

For these investigations, films were grown on semi-insulating (001) GaAs substrates using Ga, Al, As_2, and Si, as described elsewhere.[8] All samples consisted of an undoped GaAs buffer (500 nm thick), followed by Si-doped layers of GaAs (500 nm thick) and an AlAs sputter-mask (50 nm thick), all grown at 580 °C. The target free carrier concentration was $1 \times 10^{18}\,cm^{-3}$, within 50% of that predicted to maximize the GaAs power factor.[9] Following growth, a portion of the film was reserved as a reference sample, while the remainder was implanted with 100 keV In^+, at an ion fluence of $3.8 \times 10^{16}\,cm^{-2}$. At this fluence, the AlAs layer is expected to be partially sputtered away.[7] To minimize channeling effects during implantation, a 7° angle of incidence with respect to the sample surface normal was utilized. During implantation, the substrate temperature was maintained at 77 K. Following implantation, RTA was performed in argon gas for 30 s at 450, 500, and 550 °C, which we will refer to as "low," "medium," and "high" T annealed films, respectively. During RTA, a GaAs proximity cap was used to minimize As out-diffusion.

Following growth and/or implantation and/or RTA, the temperature-dependence of the resistivity, $\rho(T)$, and the Seebeck coefficient, $S(T)$, were measured using a cleaved rectangular (2 mm × 10 mm) sample configuration. In addition, room temperature Hall effect measurements were performed in a van der Pauw configuration. Prior to transport measurements in either configuration, In contacts were applied and subsequently annealed at 400 °C for 2 min in an N_2 atmosphere. For measurements of $\rho(T)$, a current was passed along the rectangular samples and the corresponding voltage was measured. For measurements of $S = \Delta V/\Delta T$, a current-driven heater and a copper block were attached to the cleaved rectangles. The thermally-induced T gradients were measured with thermocouples attached to the In contacts. The thermal conductivity of the films was measured using time-domain thermoreflectance (TDTR),[10] in which a 1550 nm pump pulse is used to heat a transducer layer on the

sample surface and a 100 fs (780 nm) probe pulse is used to measure its reflectance. The time-dependence of the reflectance is then used to calculate the decay of the sample temperature, as will be discussed below. TDTR measurements were enabled by the deposition of a surface thermal transducer consisting of a 5 nm/85 nm Ni/Al layer.

To examine the microstructure of the films, cross-sectional transmission electron microscopy (TEM) specimens were prepared using conventional mechanical polishing, followed by argon ion milling at 77 K. TEM imaging and selected area electron diffraction (SAD) were carried out in a JEOL 3011 operating at 300 kV. Energy Dispersive X-Ray Spectroscopy (EDX) and high-angle annular dark field (HAADF) scanning transmission electron microscopy (STEM) were performed in a JEOL 2010 TEM operating at 200 kV.

III. RESULTS AND DISCUSSION

A. Influence of annealing temperature on microstructure

Figure 1 presents typical bright-field TEM images of GaAs:In (a) as-implanted and following RTA at (c) low, (e) medium, and (g) high temperatures. The corresponding SAD patterns are shown in Figs. 1(b), 1(d), 1(f), and 1(h). The as-implanted film consists of a 100 nm thick a-GaAs surface film, below which is crystalline GaAs. The medium (high) T annealed film consists of a 96 nm (89 nm) recrystallized GaAs layer containing stacking faults. For the low T annealed film, a 63 nm polycrystalline GaAs layer is present. SAD indicates diffracted spots with d-spacings of 2.46 Å, within 1% of the {002} interplanar spacings of In. We note that this polycrystalline structure is presumably due to the low annealing temperature, which prevents full crystallization of the amorphized layer.

Figure 2 presents typical HAADF images of GaAs:In (a) as-implanted and following RTA at (c) low, (e) medium, and (g) high temperatures. The corresponding EDX elemental maps are shown in Figs. 2(b), 2(d), 2(f), and 2(h), with In, Ga, and Al atoms labeled in green, blue, and red, respectively. EDX reveals the formation of an 85 nm thick In-rich layer following implantation. The high T annealed film shows In diffusion towards the substrate, while the medium T annealed film shows In segregating towards the surface, forming a 100 nm thick layer. For the low T annealed film, however, In-rich clusters ~85 nm in diameter are observed, consistent with the In diffraction spots in Fig. 1(d).

For the low T annealed film, we further examined the microstructure using bright- /dark-field and high-resolution

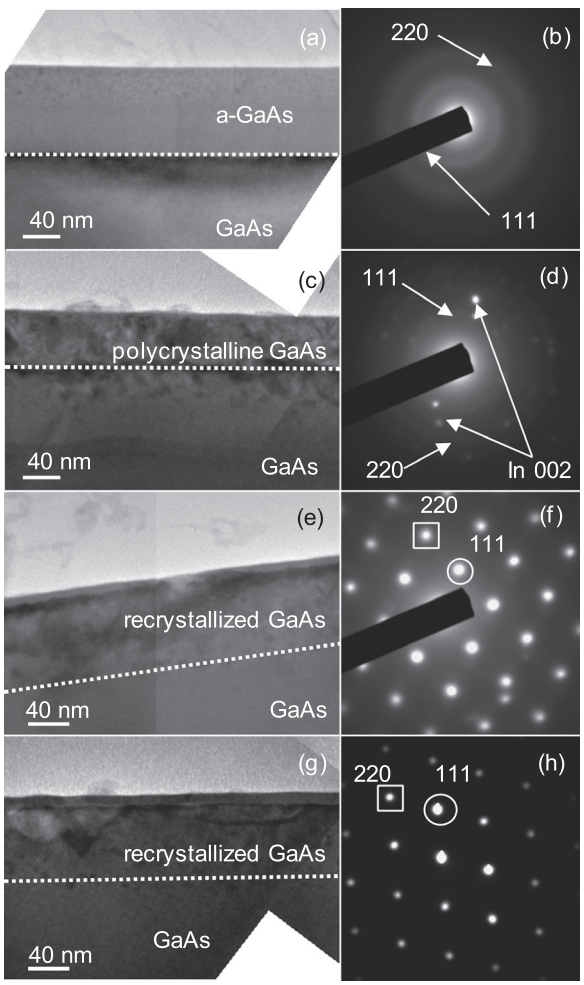

FIG. 1. Bright-field TEM images of GaAs:In (a) as-implanted, and following RTA at (c) low T, (e) medium T, and (g) high T. The corresponding SAD patterns, collected from the a-GaAs of (a) and the recrystallized layer of (c), (e), and (g), are presented in (b), (d), (f), and (h), respectively.

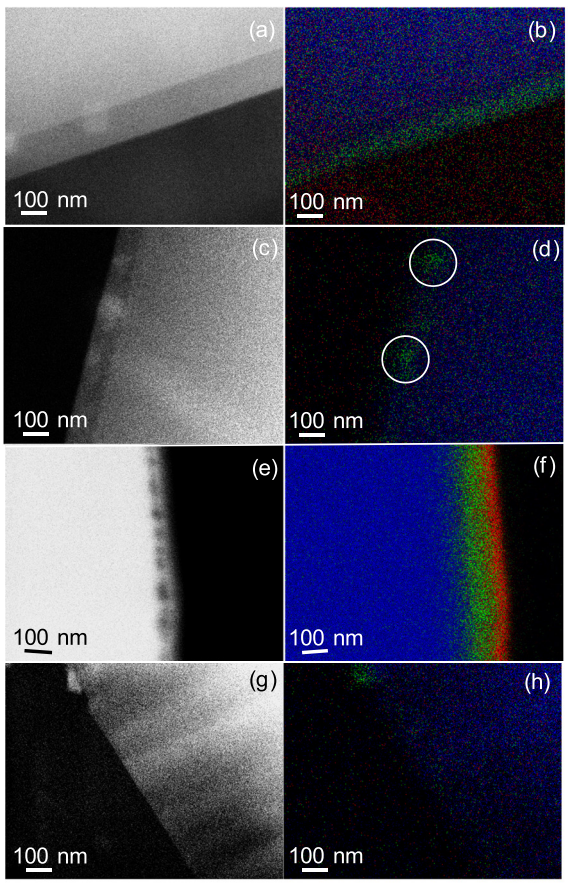

FIG. 2. Cross-sectional HAADF STEM images of GaAs:In (a) as-implanted, and following RTA at (c) low T, (e) medium T, and (g) high T. The corresponding composite elemental maps of Ga (blue), Al (red), and In (green) collected from (a), (c), (e), and (g) are presented in (b), (d), (f), and (h), respectively. The In NCs in (d) are circled as a guide to the eye.

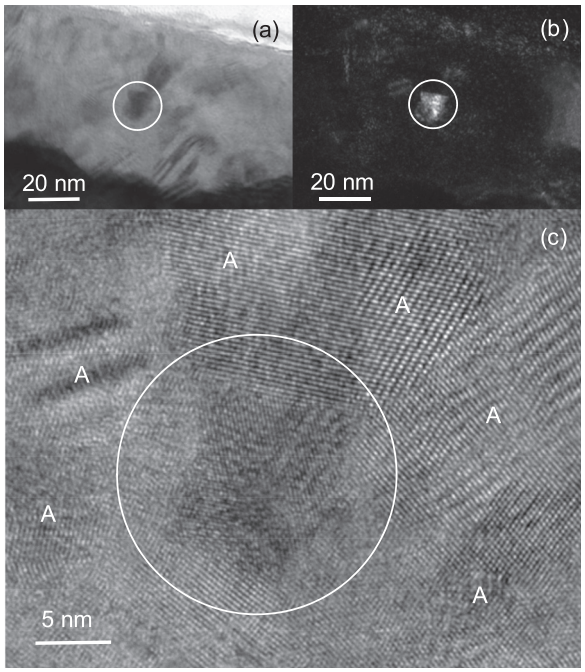

FIG. 3. Transmission electron microscopy (TEM) images of GaAs:In films following low T RTA: (a) bright-field, (b) In {110} dark-field, and (c) high resolution. An opaque 13 nm diameter feature is shown in the bright-field image in (a). In the corresponding dark-field image (b), this feature appears bright, identifying it as an In NC. In (c), the high resolution TEM image shows that the In NC is located at the boundary between GaAs crystallites, labeled "A". In (a)–(c), the In NC is circled as a guide to the eye.

TEM. In Fig. 3, close-up views of the polycrystalline GaAs layers containing In-rich clusters are shown in the (a) bright-field, (b) dark-field, and (c) high-resolution images. The dark-field image in Fig. 3(b) was obtained using the In {110} diffraction spot. A ~13 nm diameter feature is circled in Figs. 3(a)–3(c). Since the feature appears bright in Fig. 3(b), it is attributed to an In NC. We note that additional bright-field images spanning $>0.2\,\mu m^2$ reveal In NCs with sizes ranging from 10 to 20 nm. The high-resolution image in Fig. 3(c) reveals an In NC located at the boundary of multiple GaAs crystallites, labeled "A," which presumably serves as a NC nucleation site.

B. Influence of implantation and annealing on carrier concentration

We now consider the effects of RTA on the room temperature (RT) free carrier concentration, n. For the reference film, $n = 7 \times 10^{17}\,cm^{-3}$; following implantation, n decreases by ~70% to $2.0 \times 10^{17}\,cm^{-3}$, consistent with a mechanism in which point defects arising from the implantation process trap carriers and reduce n.[11] For the low T annealed film, n rises to $4.0 \times 10^{17}\,cm^{-3}$. However, the medium and high T annealed films show an increase of n to 2.4×10^{17} and $2.1 \times 10^{17}\,cm^{-3}$, respectively. It is interesting to note that the most significant increase in n occurs for the In NC-containing film, presumably due to the In NCs acting as electron donors, similar to the doping effect reported for ErAs particles in GaAs.[12]

C. Influence of In nanocrystals on thermoelectric properties

Having established the formation of In NCs and their effect on n, we now investigate the effect of these NCs on the thermoelectric properties. In Fig. 4(a), we consider $\rho(T)$ for the low T annealed film, in comparison with that of the reference film. We note that the T-dependence of ρ is similar for both the low T annealed film and the GaAs reference. For both the GaAs reference and the low T annealed film, ρ is weakly dependent on T, indicating extended-band conduction.[13] However, the low T annealed film exhibits a $\rho \sim 4.6$ times higher than the GaAs reference, due to the changes in structure and n, described above.

We have also examined the influence of the In NCs on the T-dependence of the Seebeck coefficient, $S(T)$, as shown in Fig. 4(b), in comparison with that of the reference film. At the lowest temperatures ($T < 10$ K), both films exhibit a rapid increase of $|S|$ that peaks at ~10 K. For $T > 10$ K, $|S|$ rapidly decreases until a temperature of ~100 K. This T-dependence of S is a manifestation of a strong electron-phonon interaction, often referred to as the phonon-drag effect. The T-dependence of S for these GaAs:In films is similar to that of the GaAs:In films reported previously.[7] The position of the phonon-drag peak near 10 K is similar for both the low T annealed film and the GaAs reference. In this phonon-drag regime, $|S|$ of the low T annealed film is ~190 μV/K lower than that of the GaAs reference. Presumably, the polycrystalline structure of the low T annealed film enhances phonon scattering, limiting electron-phonon interaction. For $T > 100$ K, $|S|$ increases monotonically with T, due to electron diffusion driven by the temperature gradient. In this diffusion regime, the In NC-containing film exhibits higher values of $|S|$ than those of the reference, with ~50 μV/K difference at RT. This increase in $|S|$ is presumably due to free carrier trapping at implantation-induced defects, as described above, thereby reducing n, and increasing $|S|$.

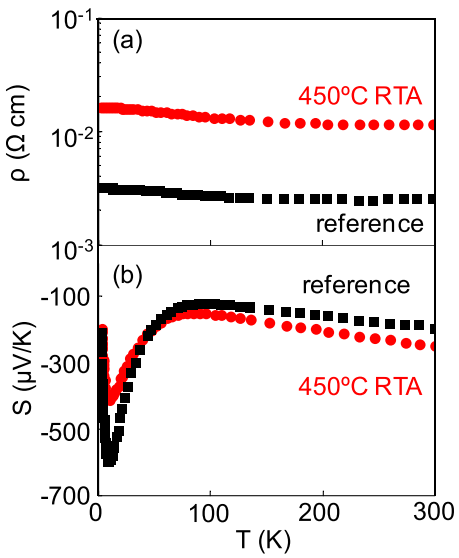

FIG. 4. (a) Resistivity, ρ, and (b) Seebeck coefficient, S, as a function of temperature for both the GaAs reference and the GaAs:In film following low T RTA.

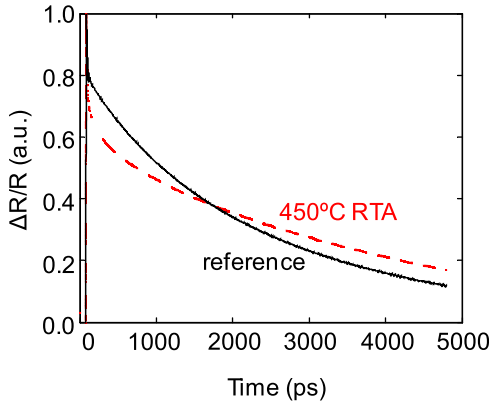

FIG. 5. Normalized transient reflectance as a function of time for the low T RTA film, in comparison to that of the GaAs reference.

We have also examined the influence of the In NCs on the thermal conductivity, κ, of the films, using an analysis of TDTR measurements. Figure 5 shows the time-dependence of the normalized reflectance for both the In NC-containing and reference GaAs films. During the first 100 ps, the metallic transducer is heated, leading to a rise in reflectance. From 200 to 4700 ps following the pump pulse, heat is dissipated through the In NC-containing (GaAs) layer in the nanocomposite (reference) film, leading to a gradual decrease in reflectance. For the analysis, we solve the time-dependent heat conduction equation,[14] assuming heat loss in the transducer and GaAs:In layers, with $\kappa_{\text{transducer}} = \kappa_{\text{Al}} = 200\,\text{W m}^{-1}\,\text{K}^{-1}$.[15] The calculated time-dependence of the reflectance is then fit with the experimental data using a least-squares minimization while varying the laser absorption depth, transducer-film boundary conductance, and κ_{film}. In all cases, the laser absorption depth lies within the thickness of the transducer layer and the thermal boundary conductance is $\sim 10^{17}\,\text{W m}^{-2}\,\text{K}^{-1}$, similar to that reported for Al/GaSb.[16] For the reference film, $\kappa_{\text{film}} = 50\,\text{W m}^{-1}\,\text{K}^{-1}$, similar to the reported value of $\kappa_{\text{GaAs}} = 55\,\text{W m}^{-1}\,\text{K}^{-1}$.[17] For the In NC-containing film, $\kappa_{\text{film}} = 26\,\text{W m}^{-1}\,\text{K}^{-1}$, ~50% of κ_{GaAs}. Thus, phonon scattering is increased in the In NC-containing film. As discussed above, In NC are often located at the boundaries of multiple GaAs crystallites. Since the density of GaAs crystallite-GaAs crystallite boundaries is higher than that of GaAs crystallite-In NC boundaries, phonons are likely primarily scattered at GaAs crystallite-GaAs crystallite boundaries.

IV. CONCLUSIONS

In summary, we examined the influence of embedded In NCs on n, ρ, S, and κ of GaAs prepared by ion implantation followed by RTA. Implantation amorphizes the surface of the GaAs film, inducing defects which trap carriers and reduce n. RTA at high and medium T results in a recrystallized GaAs film, while RTA at low T leads to a polycrystalline GaAs containing 10–20 nm diameter In NCs which act as electron donors. The GaAs crystallite boundaries serve to scatter electrons and phonons, increasing ρ and reducing κ. Furthermore, the room temperature Seebeck coefficient exhibits a 25% increase, presumably due to carrier trapping. Together, these data reveal that In NCs enhance n and S while decreasing σ. It is anticipated that application of this approach to more heavily doped GaAs layers will lead to further increases in S and σ.

ACKNOWLEDGMENTS

This research was supported by the Center for Solar and Thermal Energy Conversion, an Energy Frontier Research Center funded by the U.S. Department of Energy, Office of Science, Office of Basic Energy Science under Award Number DE-SC0000957. J.C.C. was supported in part by the AFOSR through the MURI program under Contract No. FA9950-08-1-0340. E.M. was supported by the National Science Foundation through the Materials Research Science and Engineering Center at the University of Michigan, grant DMR-1120923.

[1]L. D. Hicks, T. C. Harman, X. Sun, and M. S. Dresselhaus, Phys. Rev. B **53**, R10493 (1996).
[2]R. Venkatasubramanian, E. Siivola, T. Colpitts, and B. O'Quinn, Nature **413**, 597 (2001).
[3]M. Zebarjadi, G. Joshi, G. Zhu, B. Yu, A. Minnich, Y. Lan, X. Wang, M. Dresselhaus, Z. Ren, and G. Chen, Nano Lett. **11**, 2225 (2011).
[4]S. V. Faleev and F. Léonard, Phys. Rev. B **77**, 214304 (2008).
[5]X. Weng, W. Ye, S. J. Clarke, R. S. Goldman, V. Rotberg, A. Daniel, and R. Clarke, J. Appl. Phys. **97**, 064301 (2005).
[6]A. W. Wood, R. R. Collino, P. T. Wang, Y. Q. Wang, and R. S. Goldman, Appl. Phys. Lett. **100**, 203113 (2012).
[7]M. V. Warren, A. W. Wood, J. C. Canniff, F. Naab, C. Uher, and R. S. Goldman, Appl. Phys. Lett. **100**, 102101 (2012).
[8]B. Lita, S. Ghaisas, R. S. Goldman, and M. R. Melloch, Appl. Phys. Lett. **75**, 4082 (1999).
[9]N. Mingo, Appl. Phys. Lett. **84**, 2652 (2004).
[10]V. A. Stoica, Y.-M. Sheu, D. A. Reis, and R. Clarke, Opt. Express **16**, 2322 (2008).
[11]R. Coates and E. W. Mitchell, J. Phys. C **5**, L113 (1972).
[12]J. M. Zide, D. O. Klenov, S. Stemmer, A. C. Gossard, G. Zeng, J. E. Bowers, D. Vashaee, and A. Shakouri, Appl. Phys. Lett. **87**, 112102 (2005).
[13]M. L. Lovejoy, M. R. Melloch, and M. S. Lundstrom, Appl. Phys. Lett. **67**, 1101 (1995).
[14]R. J. Stevens, A. N. Smith, and P. M. Norris, J. Heat Transfer **127**, 315 (2005).
[15]F. Cverna, *ASM Ready Reference: Thermal Properties of Metals* (ASM International, 2002), p. 341.
[16]P. E. Hopkins, J. C. Duda, S. P. Clark, C. P. Hains, T. J. Rotter, L. M. Phinney, and G. Balakrishnan, Appl. Phys. Lett. **98**, 161913 (2011).
[17]R. O. Carlson, G. A. Slack, and S. J. Silverman, J. Appl. Phys. **36**, 505 (1965).